**Natural Hazards and Earth System Sciences**

Open Access

Discussions

# Large-scale numerical modeling of hydro-acoustic waves generated by tsunamigenic earthquakes

C. Cecioni[1], A. Abdolali[1], G. Bellotti[1], and P. Sammarco[2]

[1]Roma Tre University, Engineering Department, Via Vito Volterra 62, 00146 Rome, Italy
[2]University of Rome Tor Vergata, Civil Engineering Department, Via del Politecnico 1, 00133 Rome, Italy

Correspondence to: C. Cecioni (claudia.cecioni@uniroma3.it)

Discussion Paper | Discussion Paper | Discussion Paper | Discussion Paper |

**NHESSD**

2, 4629–4658, 2014

**Large-scale numerical modeling of hydro-acoustic waves**

C. Cecioni et al.

Title Page

| Abstract | Introduction |
| Conclusions | References |
| Tables | Figures |

◀◀   ▶▶

◀   ▶

Back   Close

Full Screen / Esc

Printer-friendly Version

Interactive Discussion

Full Screen / Esc

Printer-friendly Version

Interactive Discussion

## Abstract

Tsunamigenic fast movements of the sea-bed generate pressure waves in weakly compressible sea water, namely hydro-acoustic waves, which travel at the sound celerity in water (about $1500\,\mathrm{m\,s^{-1}}$). These waves travel much faster than the counter part long free-surface gravity waves and contain significant information on the source. Measurement of hydro-acoustic waves can therefore anticipate the tsunami arrival and significantly improve the capability of tsunami early warning systems. In this paper a novel numerical model for reproduction of hydro-acoustic waves is applied to analyze the generation and propagation in real bathymetry of these pressure perturbations for two historical catastrophic earthquake scenarios in Mediterranean Sea. The model is based on the solution of a depth-integrated equation and therefore results computationally efficient in reconstructing the hydro-acoustic waves propagation scenarios.

## 1 Introduction

Submarine earthquakes are the major cause of generation of tsunami. A correct modeling of the wave field generated by sea-bed movement is mandatory to understand the physics of the tsunami and its propagation. A sudden movement of the seabed, triggered by underwater earthquake, compresses the water column and generates pressure waves (hydro-acoustic waves) that propagate in the sea at the celerity of sound in water. Since the hydro-acoustic waves travel much faster than the surface waves, their real-time recording allows to anticipate the arrival of the tsunami. Moreover, the hydro-acoustic wave signals contain significant information on the tsunamigenic source (Cecioni et al., 2014; Chierici et al., 2010), therefore the complete modeling of these waves could in principle dramatically improve the effectiveness of tsunami early warning systems (TEWS).

The earlier studies on the tsunami evolution in weakly compressible water have been carried out by Miyoshi (1954), Sells (1965) and Yamamoto (1982). Later, analytical

studies have solved the potential fluid problem in weakly compressible water, with fast rising motion of the sea bed (Nosov, 1999; Stiassnie, 2010; Chierici et al., 2010). The analytical models, although extremely useful to investigate the features of hydro-acoustic wave generation and propagation processes, are not suited for reproduction of such phenomena at real-geographical scale. The numerical solution of the 3-D problem (Nosov and Kolesov, 2007; Bolshakova et al., 2011) is straightforward to obtain, but requires unacceptable computational time when applied to large areas. A depth-integrated equation has therefore been proposed by Sammarco et al. (2013), which reproduces the mechanics of propagation of low-frequency hydro-acoustic waves due to a sudden bottom displacement associated with earthquakes. The wave simulation by means of this equation, overcomes the computational difficulties of three-dimensional models and retains all the physical features of the phenomena.

In this paper the results and the physical implications of the first large geographical scale application of the numerical model based on the depth-integrated equation of Sammarco et al. (2013) are illustrated. The model is applied to simulate the hydro-acoustic wave propagation generated by two main tsunamigenic destructive historical earthquakes occurred in the Mediterranean sea: the AD 365 Crete event and the 1693 Sicily event. The depth-integrated model has been validated through comparison with the solution of the full three-dimensional weakly compressible wave problem in real-bathymetry, along vertical sections of the sea. The comparison allowed to set up some computational parameters in order to optimize the depth-integrated model.

The simulation of hydro-acoustic waves propagation in real bathymetry enables to investigate the correlation between these pressure waves and the generation mechanism, the source location, the bottom topography and the depth of the pressure recording point. Moreover, in the portion of Mediterranean sea considered in the present research, two deep-sea observatories are located off-shore the East Sicilian coast. These observatories, described later in more details, are equipped, among others instruments, with low-frequency and large-bandwidth hydrophones. Therefore the

numerically reproduced scenario provide indications on the attended hydro-acoustic signals in the case of submarine earthquake occurrence.

The paper is structured as follows: Sect. 2 deals with the description of the numerical model; Sect. 3 describes the large scale numerical simulations of the two selected historical tsunamis; in Sect. 4 discussions and conclusions are given.

## 2   Description of the numerical model

Consider the problem of wave propagation in weakly compressible inviscid fluid, where waves are generated by a sea-bed motion. The governing equation and boundary conditions for the fluid potential $\Phi(x, y, z, t)$ are:

$$
\begin{cases}
\Phi_{tt} - c_s^2 \nabla^2 \Phi - c_s^2 \Phi_{zz} = 0 \\
\Phi_{tt} + g\Phi_z = 0 & \text{at } z = 0 \\
\Phi_z + \nabla h \cdot \nabla \Phi + h_t = 0 & \text{at } z = -h(x, y, t)
\end{cases}
\tag{1}
$$

where $\nabla$ and $\nabla^2$ are respectively the gradient and the Laplacian in the horizontal plane $x, y$, while subscript with the independent variables denotes partial derivatives, $c_s$ is the celerity of sound in water, $g$ is the gravity acceleration. $h$ is the water depth, given by the rest bottom topography $h_b(x, y)$ net of the earthquake bottom motion $\zeta(x, y, t)$

$$
h(x, y, t) = h_b(x, y) - \zeta(x, y, t).
\tag{2}
$$

From Eq. (2) the water depth time-variation $h_t$ is zero everywhere except on the earthquake zone,

$$
h_t = -\zeta_t = -\frac{\zeta_0}{\tau} [H(t) - H(t - \tau)],
\tag{3}
$$

where $H$ is the Heaviside step function, $\zeta_0(x, y)$ is the residual displacement, $\tau$ is the duration of the sea-bed motion and the sea-bed velocity is assumed constant, as $\zeta_0/\tau$.

The solution of Eq. (1) is given by an infinite sum of natural modes, $n = 0, 1, \ldots$ (Eyov et al., 2013). The first mode ($n = 0$) represents the gravity surface wave, i.e. the tsunami; the other modes ($n \geq 1$), namely the hydro-acoustic modes, are responsible of elastic oscillations of the water body. The hydro-acoustic waves are characterized by a set of natural frequencies, namely cut-off frequencies:

$$f^{(n)} = \frac{(2n-1)c_s}{4h} \tag{4}$$

where $n \geq 1$ is the indicator of the hydro-acoustic mode. Evanescent and progressive waves are associated respectively to lower and higher frequencies than the cut-off ones (Eq. 4).

Sammarco et al. (2013) via a proper application of the averaging technique to the problem (Eq. 1), in the hypothesis of constant $c_s$ and mild sloped sea-bed ($\nabla h \ll kh$), found a depth-integrated equation, which in hyperbolic form reads:

$$\psi_{n_{tt}} \left( \frac{C_n}{c_s^2} + \frac{1}{g} \right) - \nabla \left( C_n \nabla \psi_n \right) + \left( \frac{\omega^2}{g} - \beta_n^2 C_n \right) \psi_n = h_t D_n \tag{5}$$

where $\psi(x, y, t)$ is the fluid velocity potential at the undisturbed free-surface. Equation (5) has been named Mild-Slope Equation in Weakly Compressible fluid (MSEWC). The subscript $n$ indicates that Eq. (5) is valid for the generic $n$th mode (hydro-acoustic and gravity). Superimposition of the solutions of Eq. (5) for each mode will lead to complete modeling of the fluid potential, $\Phi(x, y, z, t) = \sum_{n=0}^{\infty} \psi_n(x, y, t) f_n(z)$, generated by a fast sea-bed motion, where the $f_n$'s are the classic eigenfunctions of the constant depth homogeneous problem, which is valid for mild-sloped sea bed

$$f_n(z) = \frac{\cosh[\beta_n(h+z)]}{\cosh(\beta_n h)}. \tag{6}$$

In Eq. (5) $\beta_n$'s are the roots of the dispersion relation

$$\beta_n = \begin{cases} n = 0 & \beta_n = \beta_0 & \omega^2 = g\beta_0 \tanh(\beta_0 h) \\ n \geq 1 & \beta_n = i\overline{\beta_n} & \omega^2 = -g\overline{\beta_n} \tan\left(\overline{\beta_n} h\right) \end{cases} \tag{7}$$

while the terms $C_n(x,y)$ and $D_n(x,y)$ are given by

$$C_n(x,y) = \int_{-h}^{0} f_n^2 \, dz = \frac{2\beta_n h + \sinh(2\beta_n h)}{4\beta_n \cosh^2(\beta_n h)} \tag{8}$$

$$D_n(x,y) = \frac{1}{\cosh^2(\beta_n h)} \frac{\int_{-h}^{0} f_n \, dz}{\int_{-h}^{0} f_n^2 \, dz} = \frac{4 \tanh(\beta_n h)}{(2\beta_n h + \sinh(2\beta_n h))}. \tag{9}$$

More details on the wave derivation can be found in Sammarco et al. (2013). Note that for incompressible fluid, i.e. in the limit $c_s \longrightarrow \infty$, Eq. (5) reduces to the classical MSE. In the time domain the MSEWC reproduces the fluid potential characteristic of a narrow frequency banded wave spectrum, around the value of a carrier frequency, which determines the variables $\beta_n$, $C_n$ and $D_n$. For each narrow frequency band of the wave spectrum, Eq. (5) is solved and then the results are superimposed.

The numerical model makes use of the Finite Element Method, and solves the hyperbolic equation by means of a time-marching numerical scheme. The model uses the Generalized-$\alpha$ method, which is a one-step implicit method for solving the transient problem. The method, first developed for the second-order equations in structural mechanics (Chung and Hulbert, 1993; Jansen et al., 2000), increases the amount of numerical damping present without degrading the order of accuracy.

**Large-scale numerical modeling of hydro-acoustic waves**

C. Cecioni et al.

## 3 Mediterranean tsunami scenarios

Two historical tsunami scenarios have been reproduced by means of the numerical solution of the depth-integrated MSEWC (Eq. 5). The selected tsunamis events are those generated by the AD 365 Crete earthquake and the 1693 Sicily earthquake. We refer to the paper of Tonini et al. (2011), which estimates the tsunami hazard for the city of Catania (Sicily, Italy) by means of the Worst-case Credible Tsunami Scenario Analysis (WCTSA) technique. The authors have considered several possible earthquake scenarios of the two events of AD 365 and 1693, and performed a sensitivity analysis on the source size, since the choice of the source strongly affects the final results in terms of inundation map. The historical tsunami analyzed in the present study have been selected among the ones proposed by Tonini et al. (2011), as those generated by the largest reconstructed submerged earthquakes. Their seismic parameters are reported in Table 1. Figure 1 shows the domain of application of the numerical model, which is a portion of the Mediterranean Sea, and the relative bathymetry. The boundaries are the coasts of Italy, Greece and North Africa. Dashed black lines represent the open sea boundaries, where a condition of waves free exit is imposed. For the 1693 Sicily tsunami scenario the numerical domain is restricted to the portion of Mediterranean Sea bounded by the thin dashed line. The data of the Mediterranean Sea bathymetry, represented in Fig. 1, are taken from ETOPO1, a 1 min bathymetric and relief database of the National Geophysical Data Center (NGDC). In Fig. 1 two points are indicated, namely CTS and CP, which correspond to the position of two submarine observatories, equipped with hydrophones. The Catania Test Site (CTS) observatory (37°30.008′ N, 15°23.034′ E, North site, 37°32.861′ N, 15°23.844′ E, South site) is located around 25 km offshore the harbor of Catania and at a water depth of 2 km. The Capo Passero (CP) observatory (36°17′33.57″ N, 15°58′53.02″ E), is located 100 km offshore the Capo Passero village and at 3500 m below the mean sea level. Both observatories are connected to shore through a submarine electro-optical cable. The observatories located in the Catania Test Site are dedicated to multi-disciplinary

activities, equipped with low-frequency (0.1 Hz–1 kHz) and large-bandwidth (10 Hz–70 kHz) hydrophones, seismometers, CTDs, magnetometers and current-meters. The Capo Passero submarine observatory has been designed and constructed by INFN in the framework of the NEMO and KM3neT-Italia (www.km3net.org) projects. Aboard this observatory an antenna of large bandwidth hydrophone (10 Hz–70 kHz) has been installed within the activities of the SMO (Submarine Multidisciplinary Observatory) FIRB research project, funded by the Italian Ministry for University and Scientific Research (MIUR). SMO aims at collecting real-time acoustic data for three main scientific areas: astrophysics, for the neutrino detection, bio-acoustics, for the whale tracking and geophysics for the recording of hydro-acoustic wave generated by submerged earthquakes. The SMO has been installed in March 2013 and since then has been acquiring data in real time. The position of the two observatories has been used to analyze the numerically reproduced hydro-acoustic signals generated by the two historical earthquakes. Details on each earthquake-tsunami event and their modeling, are given in the following subsections.

## 3.1 The AD 365 scenario

The AD 365 earthquake was an undersea earthquake occurred on 21 July AD 365 in the Eastern Mediterranean, with an assumed hypo-center located off western Crete, along a major thrust fault parallel to the western Hellenic trench. Geologists today estimate that the quake intensity was 8.5 on the Richter Scale or higher, causing widespread destruction in central and southern Greece, Libya, Egypt, Cyprus, and Sicily. In Crete nearly all towns were destroyed. This earthquake was followed by a tsunami which devastated the Mediterranean coasts, killing thousands of people and hurling ships 3 km inland.

This work considers a reconstructed scenario of this earthquake, in order to numerically reproduce the generated hydro-acoustic waves. Following the works of Shaw et al. (2008) and Tonini et al. (2011), we consider almost the whole rupture of the western Hellenic arc. Making use of the simplified fault model of Tonini et al. (2011), the seismic

parameters are described in Table 2. The reconstructed residual sea-bed dislocation, $\zeta_0$ has been calculated by means of the Okada (1985) formulas and it is shown in Fig. 2.

In Fig. 2 two straight lines $AB$ and $CB$ are drawn: they pass through the locations of the submarine observatories of Catania (CTS) and Capo Passero (CP). Along these two lines the MSEWC (Eq. 5) has been solved and compared with the solution of the complete 3-D problem (Eq. 1) applied to the vertical sections ($AB$ and $CB$). Figure 3 shows the water depth (upper panels) and the sea-bed residual vertical dislocations (lower panels) along these two cross sections. The comparison at the two cross sections reveals very good agreement between the depth-integrated and the 3-D models. For sake of brevity just the results at the two points, CTS and CP, are presented in Fig. 4. The panels $a$ and $b$ represent respectively the free-surface elevation time series and their frequency spectra at the CTS point; while the panels $c$ and $d$ are relative to the CP point. In each panel the upper plots show the solution of the 3-D reference model, and the lower plots show the depth-integrated model results. The time series are in very good agreement, although, as can be noted from their spectra (right column), not all the frequencies have been reproduced in the solution of the depth-integrated equation. In particular for the simulation here presented a set of MSEWC has been solved, each one relative to a frequency in the range $f = 0.1$–$0.5$ Hz, with a $\Delta f = 0.04$ Hz.

The comparison results have been used to set up some computational parameters of the large scale simulation and to optimize the number of frequencies and number of modes to solve in order to obtain a good reproduction of the hydro-acoustic signal, minimizing the computational costs. For the AD 365 earthquake scenario in the whole domain, the frequencies range $f = 0.1$–$0.5$ Hz, with a $\Delta f = 0.04$ Hz, has been evaluated as sufficient in order to accurately reproduce the hydro-acoustic waves. It has been found that the first acoustic mode alone is responsible of carrying most of the energy transferred from the sea-bed motion. The large geographical simulations has been carried out in the domain of Fig. 1, which has been discretized by 2 250 000 triangular

elements, using a maximum element mesh size of 1200 m. In order to reproduce the hydro-acoustic waves propagation in the whole domain, the simulation cover a time of 720 s, with a time step of 0.1 s. The computational time was about 100 h on a high-speed computer equipped with 12 cores i7 3.20 GHz CPU and 64 GB RAM.

The results of the numerical model application in terms of free-surface elevation are represented in Fig. 5. At the time $t = 0$ the earthquake occurs, then the hydro-acoustic wave travels in the Mediterranean sea at the sound celerity in water, assumed constant as 1500 m s$^{-1}$. Each 90 s a snapshot of the free-surface elevations is represented, showing that after 180 s the coasts of Libya (Africa) are reached by the hydro-acoustic waves, while after 360 s the acoustic signal arrives at the coasts of Tunisia and Italy. After about 500 s the hydro-acoustic perturbation has covered almost all the domain. From the snapshots for $t > 450$ s it can be noted that the maximum values of free-surface oscillation are located around the areas of deeper waters, which occur, as can be seen in Fig. 1, south of Greece and between Sicily and Libya, in the middle of the numerical domain. The simulation results shown in Fig. 5, confirm that the hydro-acoustic signal do not propagate up-slope (Nosov and Kolesov, 2007; Kadri and Stiassnie, 2012), i.e. the shallower water area as south-west of Sicily are not reached by the hydro-acoustic perturbation even after longer time from the earthquake occurrence.

At the two points where the submarine stations are located, CTS and CP, the simulated pressure perturbations associated to hydro-acoustic first mode, are calculated at the sea-bottom. Figure 6 represents the pressure time series (left column) and the frequency spectra (right column) at Catania Test Site submarine station (upper plots) and at Capo Passero submarine station (lower plots). At both points the hydro-acoustic signal arrives around 5 min after the earthquake occurrence, while the long free-surface tsunami waves arrive after about 40 min, assuming a constant velocity of $\sqrt{gh}$ in a mean water depth of 2.5 km.

Since most of the sea-bed motion occurs at a water depth of 3 km, the generated hydro-acoustic waves oscillate at a frequency close to the cut-off value of the first

hydro-acoustic mode, i.e. $f^{(1)} = c_s/4h = 0.12$ Hz. This signal is however filtered when traveling on shallower water depth, which allow the propagation only of higher frequency waves (Kadri and Stiassnie, 2012). The model results, shown in term of frequency spectra in Fig. 6, confirm this water depth filtering effect: the CTS is located at a water depth of 2 km and therefore the cut-off frequency for propagating wave is $f^{(1)} = 0.19$ Hz; the CP site is located at 3 km of water depth and records wave oscillation of 0.12 Hz.

## 3.2 The 1693 scenario

On 11 January 1693 a powerful earthquake occurs offshore the East coast of Sicily, Italy. This earthquake was preceded by a damaging fore-shock on 9 January. It had an estimated magnitude of 7.2, one of the most powerful in Italian history, destroying at least 70 towns and cities and causing the death of about 60 000 people. The earthquake was followed by tsunamis that devastated the coastal villages at the Ionian Sea coasts and in the Strait of Messina (Tinti et al., 2001). The strongest effects were concentrated around Augusta, where the initial withdrawal of the water left the harbor dry, followed by a wave of at least 2.4 m height, possibly as much as 8 m, that inundated part of the town. The maximum inundation of about 1.5 km was recorded at Mascali. The identification of the tsunami source is still an open issue; Tonini et al. (2011) carried out the Worst-case Credible Tsunami Scenario Analysis on the basis of a possible earthquake and a possible submerged landslide. For the analysis of the hydro-acoustic wave generation, the reconstructed earthquake scenario assumed by Tonini et al. (2011) has been chosen. The seismic parameters of Table 3 are taken as wave generation condition. Figure 7 shows the plan distribution of the vertical residual sea-bed motion in the overall numerical domain, which occurs downward, differently from the AD 365 Crete scenario.

Again, the depth-integrated model is tested by comparison with the 3-D solution at two vertical sections of the sea. The position of these sections is represented in

Fig. 7, while Fig. 8 shows the water depth and the vertical residual sea-bed dislocation over the two sections. From the comparison between the solution of the complete 3-D equation and of the MSEWC, a good agreement is found over all the points of both sections. The results at Capo Passero site on the FG section and at a point close to the Greek coast (point P) on the DE section, are presented.

Figure 9 shows free-surface elevation time series and frequency spectra at CP point (panels a and b) and at P point, close to the Greek coast (panels c and d). In each panel the upper plot shows the 3-D reference model results, while the lower panel shows the solution of the MSEWC. The depth-integrated results in the time domain almost perfectly reproduce the solution of the 3-D mathematical problem. As it can be noted by looking at the spectra, the comparison is in a good agreement for the MSEWC reproduced frequency range (0.15–0.3 Hz). In the depth-integrated modeling the reproduction of frequencies out of this range, and relative to the second and higher hydro-acoustic mode, increases the computational time without providing a relevant improvement in the wave simulation. From the complete 3-D simulation it is possible to notice clearly that the hydro-acoustic signal, during its propagation vibrates at the normal frequencies of the water layer where it has been generated, around 2 km. The Capo Passero observation site is at a water depth of about 3 km, deeper than the earthquake location and close to it, therefore the frequency spectrum at CP of Fig. 9 shows five peaks, which are relative to the first five hydro-acoustic modes, that occur at the normal frequencies $f^{(n)}$ = 0.19, 0.56, 0.9, 1.31 and 1.69 Hz, accordingly to Eq. (4). Traveling far from the generation area the pressure perturbation looses this peaked frequency spectrum around the cut-off values, as can be noted at point P, around 350 km far from the earthquake.

The large scale depth-integrated simulation has been carried out in the domain represented in Fig. 7, which has been discretized by means of triangular elements with a maximum size of 1200 m, for a total of 1 110 000 elements. The time interval numerically reproduced is of 600 s after the earthquake occurrence and a time step of 0.1 s

has been used. The computational time to reproduce this simulation was about 50 h using the same computer described before.

Snapshots of the free-surface elevation from $t = 0$ (earthquake occurrence) every 1 min, up to 8 min, are shown in Fig. 10. At time $t = 4$ min the hydro-acoustic wave has reached the Greek coasts. After that time, the maximum values of the free-surface hydro-acoustic waves, around 6 cm, are at the deeper waters, while the propagation in the shallower areas does not occur.

The results of the large scale depth-integrated simulation are presented at the two observation points, CTS and CP, in terms of bottom pressure. Figure 11 shows the pressure signals in the time and the frequency domain, at the two points CTS (upper plots) and CP (lower plots). The CTS point lies above the earthquake, while CP point is about 100 km distant from the epicenter: hence the hydro-acoustic signal arrives after about 1 min from the earthquake occurrence. Despite the time of arrival and a greater amplitude of the waves at CTS just after the earthquake occurrence, the two pressure signals are very similar. The generated signal has a peak frequency around 0.19 Hz, since the waves are generated at a water depth of 2 km, and at the same frequency are associated propagating modes at the deeper 3 km water depth (CP).

## 4  Discussion and conclusions

The Mediterranean sea-bed is affected by intense seismic activities (Tinti et al., 2004). The potential tsunamis can therefore be destructive since the coasts are densely populated and very close, i.e. the travel time of tsunami wave towards the coast is in the order of few minutes up to one hour. A rapid detection of the tsunami generation in this region is mandatory for a future development of early warning systems and the use of the hydro-acoustic signals can cope with this necessity. The proposed model reproduces the mechanism of propagation of hydro-acoustic waves due to a sudden bottom displacement associated with earthquakes, solving the Mild-Slope Equation in Weakly Compressible fluid of Sammarco et al. (2013). In order to develop innovative

warning procedures based on these acoustic signals, the correct modeling of wave field, in weakly compressible fluid, at real-scale domains is extremely important. The use of a depth-integrated equation allows the simulation in large geographical areas, as the Mediterranean Sea, where the 3-D modeling require huge computational times.
The depth-integrated equation has been already validated by Sammarco et al. (2013); however in this paper a first application and validation in real bathymetry has been developed. The full modeling of the hydro-acoustic waves field generated by two historical tsunamigenic earthquake scenarios in the Mediterranean Sea, has been carried out.

The numerical model results highlight that the sea-bed motion energy is transferred to hydro-acoustic waves mainly at the frequencies just after the cut-off values of each acoustic mode. Close to the generation area the frequency spectra clearly show energy peaks for each acoustic mode; while during wave propagation the hydro-acoustic energy will distribute along frequencies higher than the cut-off values. The simulation of the 1693 earthquake scenario shows that 100 km far from the epicenter, at Capo Passero observation site, the hydro-acoustic waves recorded still allow to identify the energy associated to each acoustic mode. The numerical simulations confirms that the first mode is the one which carries most of the energy. The hydro-acoustic modes propagate undisturbed in water layer equal or deeper than the one where they have been generated. As the waves propagate in shallower water depth, characterized by higher cut-off frequencies, the components with frequencies lower than the cut-off become evanescent: i.e. when hydro-acoustic waves propagate towards shallower sea depth, the water layer acts as a frequency filter.

To implement innovative TEWS based on measurement and analysis of hydro-acoustic signals, the complete modeling of hydro-acoustic waves in real bathymetry has proven to be extremely useful. The numerical model simulations show that the hydrophones must be placed in waters deep enough to record larger frequency range and, if possible, not shielded by sea-mounts. However these instruments should be connected to the shore by submarine cables to guarantee fast data transmission, therefore their location can not be too far from the coastline: hence the model can

help choosing the right positioning of the hydrophones system. For the portion of the Mediterranean sea here analyzed, the numerical simulation results suggest that offshore the Sicilian East coast, where the instruments have been placed, and off-shore Greek West coast, the waters are deep enough to record and identify the hydro-acoustic waves generated by seismic activities in both the Hellenic arc and the Ionian Sea (South Italy).

# References

Bolshakova, A., Inoue, S., Kolesov, S., Matsumoto, H., Nosov, M., and Ohmachi, T.: Hydroa-coustic effects in the 2003 Tokachi-oki tsunami source, Russ. J. Earth Sci., 12, ES2005, doi:10.2205/2011ES000509, 2011. 4631

Cecioni, C., Bellotti, G., Romano, A., Abdolali, A., and Sammarco, P.: Tsunami early warning system based on real-time measurements of hydro-acoustic waves, Procedia Eng., 70, 311–320, 2014. 4630

Chierici, F., Pignagnoli, L., and Embriaco, D.: Modeling of the hydroacoustic signal and tsunami wave generated by seafloor motion including a porous seabed, J. Geophys. Res.-Oceans, 115, C03015, doi:10.1029/2009JC005522, 2010. 4630, 4631

Chung, J. and Hulbert, G.: A time integration algorithm for structural dynamics with improved numerical dissipation: the generalized-$\alpha$ method, J. Appl. Mech., 60, 371–375, 1993. 4634

Eyov, E., Klar, A., Kadri, U., and Stiassnie, M.: Progressive waves in a compressible-ocean with an elastic bottom, Wave Motion, 50, 929–939, 2013. 4633

Jansen, K. E., Whiting, C. H., and Hulbert, G. M.: A generalized-$\alpha$ method for integrating the filtered Navier–Stokes equations with a stabilized finite element method, Comput. Method. Appl. M., 190, 305–319, 2000. 4634

Kadri, U. and Stiassnie, M.: Acoustic-gravity waves interacting with the shelf break, J. Geophys. Res.-Oceans, 117, C03035, doi:10.1029/2011JC007674, 2012. 4638, 4639

Miyoshi, H.: Generation of the tsunami in compressible water (Part I), J. Oceanogr. Soc. Jpn., 10, 1–9, 1954. 4630

5　Nosov, M. A.: Tsunami generation in compressible ocean, Phys. Chem. Earth B, 24, 437–441, 1999. 4631

Nosov, M. A. and Kolesov, S. V.: Elastic oscillations of water column in the 2003 Tokachi-oki tsunami source: in-situ measurements and 3-D numerical modelling, Nat. Hazards Earth Syst. Sci., 7, 243–249, doi:10.5194/nhess-7-243-2007, 2007. 4631, 4638

10　Okada, Y.: Surface deformation due to shear and tensile faults in a half-space, B. Seismol. Soc. Am., 75, 1135–1154, 1985. 4637

Sammarco, P., Cecioni, C., Bellotti, G., and Abdolali, A.: Depth-integrated equation for large-scale modelling of low-frequency hydroacoustic waves, J. Fluid Mech., 722, R6, doi:10.1017/jfm.2013.153, 2013. 4631, 4633, 4634, 4641, 4642

15　Sells, C. C. L.: The effect of a sudden change of shape of the bottom of a slightly compressible ocean, Philos. T. Roy. Soc. Lond. A, 258, 495–528, 1965. 4630

Shaw, B., Ambraseys, N., England, P., Floyd, M., Gorman, G., Higham, T., Jackson, J., Noc- quet, J.-M., Pain, C., and Piggott, M.: Eastern Mediterranean tectonics and tsunami hazard inferred from the AD 365 earthquake, Nat. Geosci., 1, 268–276, 2008. 4636

20　Stiassnie, M.: Tsunamis and acoustic-gravity waves from underwater earthquakes, J. Eng. Math., 67, 23–32, 2010. 4631

Tinti, S., Armigliato, A., and Bortolucci, E.: Contribution of tsunami data analysis to constrain the seismic source: the case of the 1693 eastern Sicily earthquake, J. Seismol., 5, 41–61, 2001. 4639

25　Tinti, S., Maramai, A., and Graziani, L.: The new catalogue of Italian tsunamis, Nat. Hazards, 33, 439–465, 2004. 4641

Tonini, R., Armigliato, A., Pagnoni, G., Zaniboni, F., and Tinti, S.: Tsunami hazard for the city of Catania, eastern Sicily, Italy, assessed by means of Worst-case Credible Tsunami Scenario Analysis (WCTSA), Nat. Hazards Earth Syst. Sci., 11, 1217–1232, doi:10.5194/nhess-11- 1217-2011, 2011. 4635, 4636, 4639, 4645, 4646, 4647, 4649, 4654

30　Yamamoto, T.: Gravity waves and acoustic waves generated by submarine earthquakes, Int. J. Soil Dyn. Earthq. Eng., 1, 75–82, 1982. 4630

Title Page

Abstract | Introduction

Conclusions | References

Tables | Figures

|◀ | ▶|

◀ | ▶

Back | Close

Full Screen / Esc

Printer-friendly Version

Interactive Discussion

Full Screen / Esc

Printer-friendly Version

Interactive Discussion

**Table 1.** Magnitude $M_w$ and seismic moment $M_0$ for the two scenarios as determined by Tonini et al. (2011).

| Scenario | $M_w$ | $M_0$ (Nm) |
|---|---|---|
| AD 365 | 8.5 | $6.32 \times 10^{21}$ |
| 1693 | 7.2 | $7.07 \times 10^{19}$ |

**Table 2.** Seismic parameters of AD 365 Crete earthquake, as reconstructed by Tonini et al. (2011), for the North segment 1 and South segment 2.

| Seismic parameters | Segment 1 | Segment 2 |
|---|---|---|
| Length (m) | 230 | 230 |
| Width (m) | 90 | 90 |
| Strike (°) | 312 | 320 |
| Dip (°) | 21 | 21 |
| Rake (°) | 90 | 90 |
| Slip (m) | 5 | 5 |
| Upper edge depth (km) | 5 | 5 |

**Table 3.** Seismic parameters of the 1693 Sicily earthquake, as reconstructed by Tonini et al. (2011), for the four segments from North to South.

| Seismic parameters | Segment 1 | Segment 2 | Segment 3 | Segment 4 |
|---|---|---|---|---|
| Length (m) | 14.7 | 8.8 | 5 | 19.2 |
| Width (m) | 16.5 | 16.5 | 16.5 | 16.5 |
| Strike (°) | 329 | 322 | 343 | 360 |
| Dip (°) | 35 | 35 | 35 | 35 |
| Rake (°) | 270 | 270 | 270 | 270 |
| Slip (m) | 3 | 3 | 3 | 3 |
| Upper edge depth (km) | 0.5 | 0.5 | 0.5 | 0.5 |
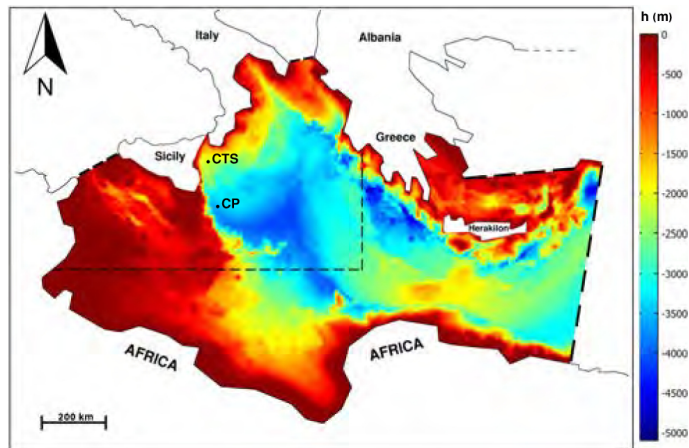
**Figure 1.** Mediterranean Sea bathymetry relative to the numerical domain.
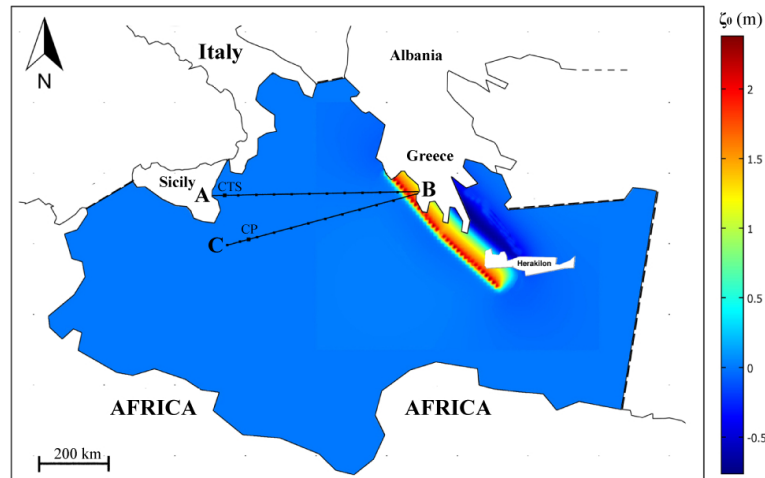
**Figure 2.** Residual vertical sea-bed dislocation, $\zeta_0$ (m), for the AD 365 Crete earthquake as reconstructed by Tonini et al. (2011).

Full Screen / Esc

Printer-friendly Version

Interactive Discussion



**Figure 3.** Upper panels: vertical sections AB and CB of Fig. 2. Section AB contains the location of the Catania submarine observatory, while section CB the Capo Passero Observatory. Lower panels: residual vertical sea bed displacement $\zeta_0$ relative to the above vertical section.
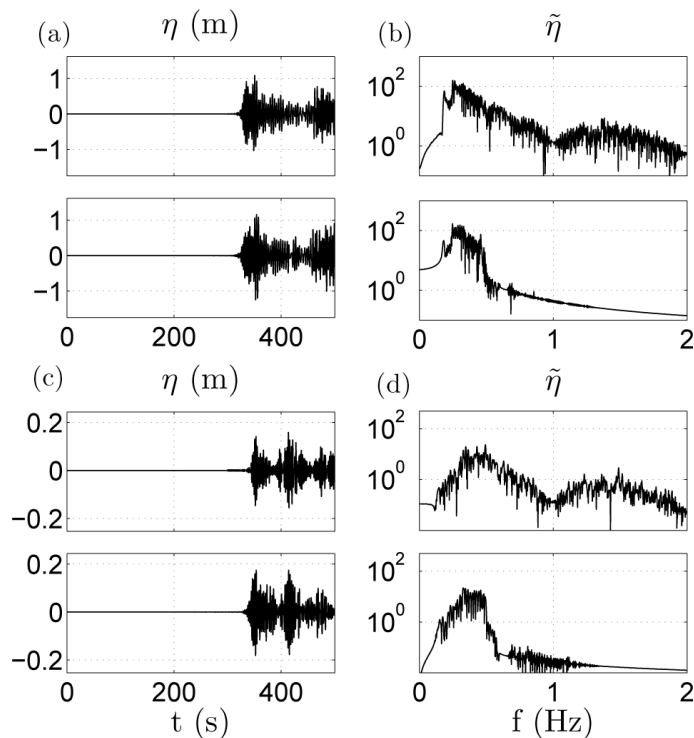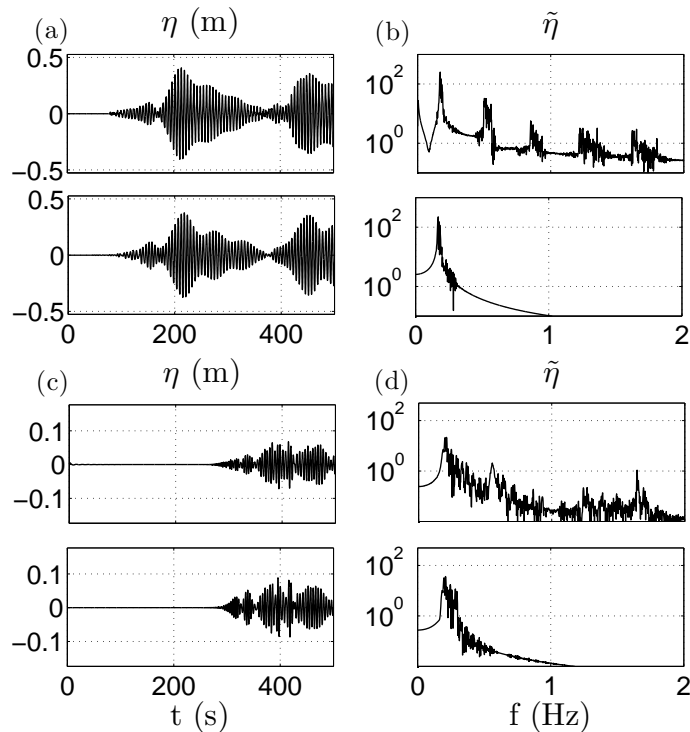
**Figure 4.** Free-surface time series (left column) and their relative frequency spectra (right column) at the CTS point (**a** and **b**) and CP point (**c** and **d**). Comparison between the solution of the 3-D reference model (upper plots) and the solution of the depth-integrated equation (lower plots).

Discussion Paper | Discussion Paper | Discussion Paper | Discussion Paper

NHESSD

2, 4629–4658, 2014

**Large-scale numerical modeling of hydro-acoustic waves**

C. Cecioni et al.

Title Page

Abstract | Introduction

Conclusions | References

Tables | Figures

|◄ | ►|

◄ | ►

Back | Close

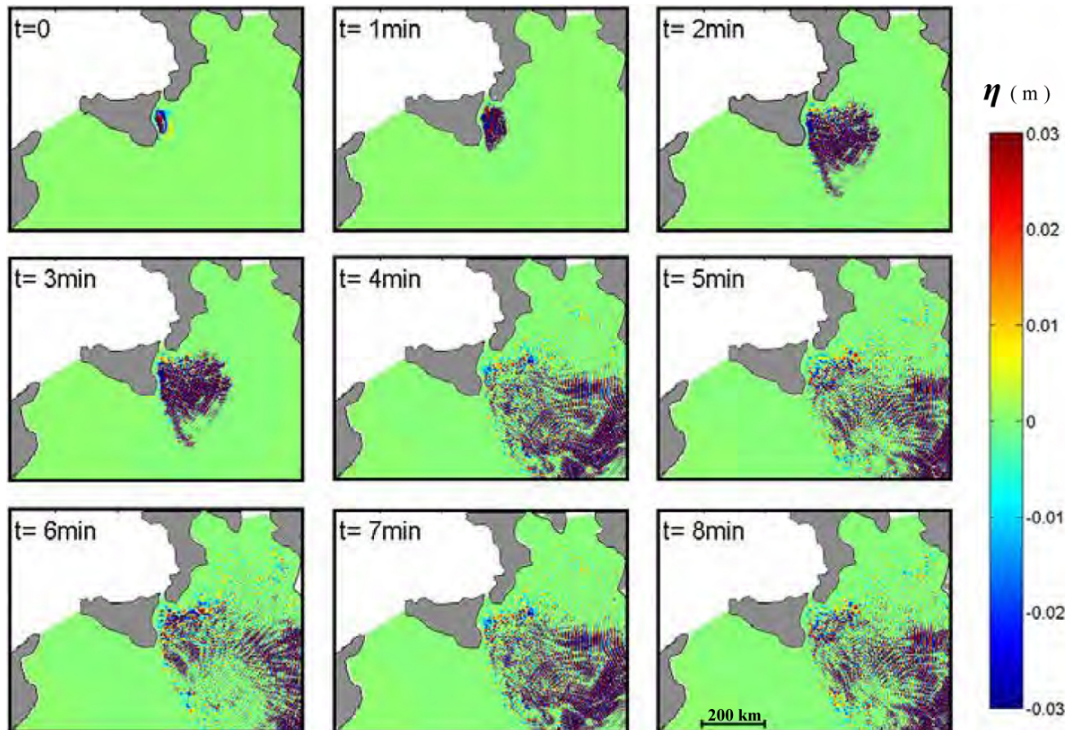Full Screen / Esc

Printer-friendly Version

Interactive Discussion
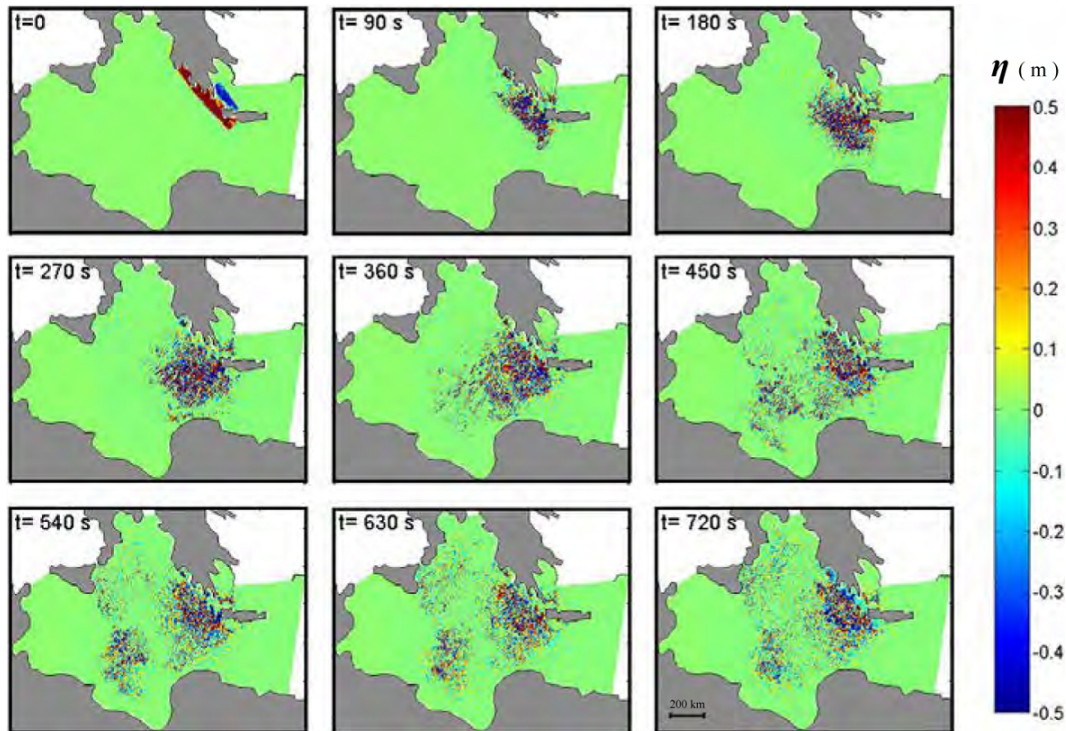
**Figure 5.** Snapshots of the free surface ($\eta$) hydro-acoustic perturbation given by the AD 365 Crete earthquake. $t = 0$ refers to the time of occurrence of the earthquake.
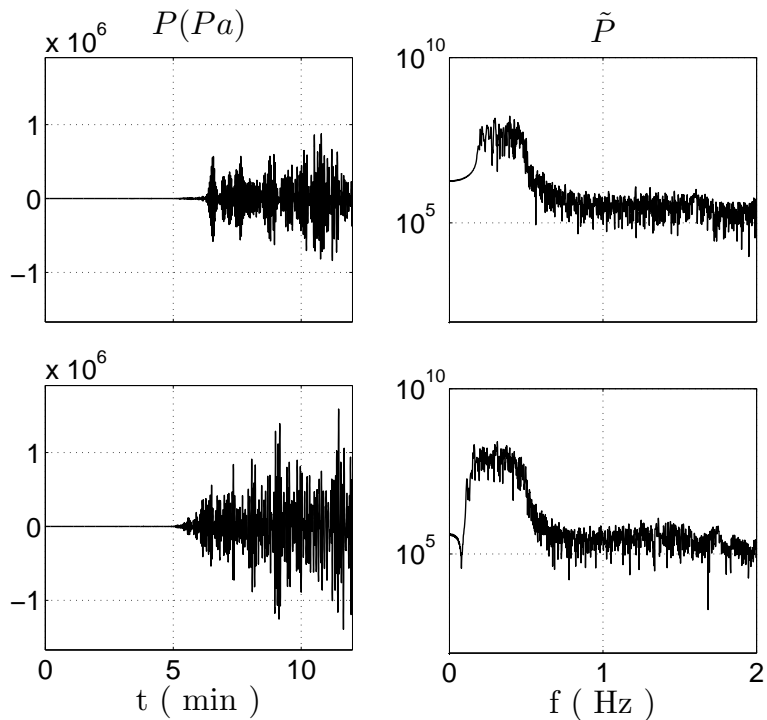
**Figure 6.** Pressure time series (left column) and their frequency spectra (right column) at Catania Test Site point (upper plots) and at Capo Passero point (lower plots), resulting from the numerical solution of the depth-integrated Eq. (5) over the whole domain.

Full Screen / Esc

Printer-friendly Version

Interactive Discussion
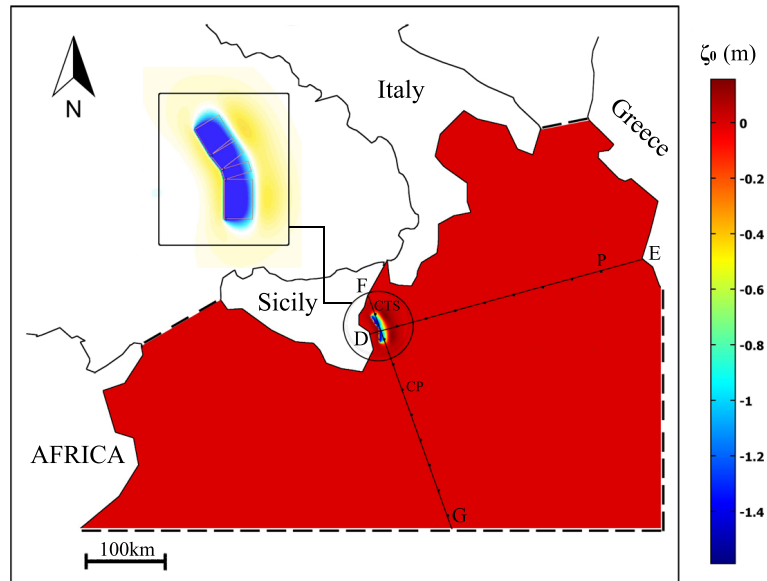


**Figure 7.** Residual vertical sea-bed dislocation, $\zeta_0$ (m), for the 1693 Sicily earthquake, as reconstructed by Tonini et al. (2011)

Title Page

Abstract | Introduction

Conclusions | References

Tables | Figures

|◄ | ►|

◄ | ►

Back | Close

Full Screen / Esc

Printer-friendly Version

Interactive Discussion
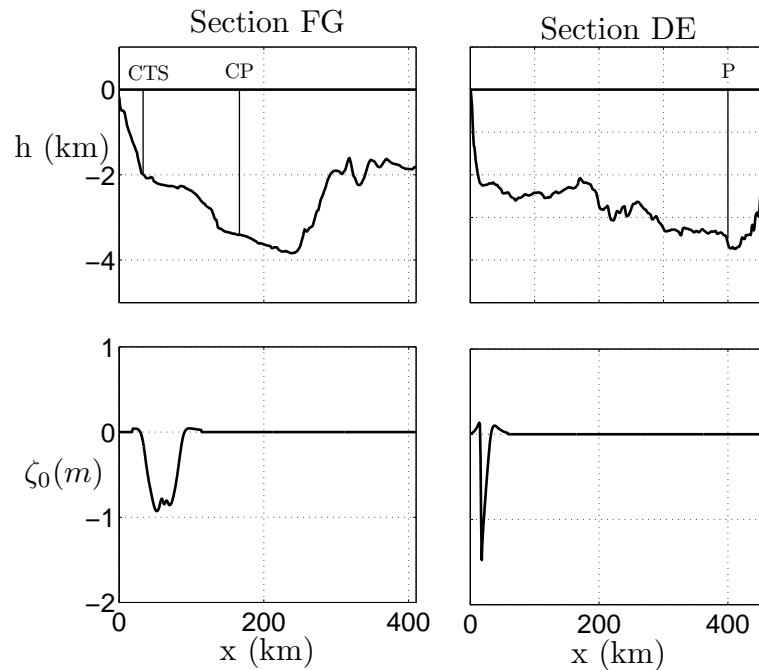
**Figure 8.** Upper panels: vertical sections FG and DE of Fig. 7. Lower panels: residual vertical sea bed displacement $\zeta_0$ relative to the above vertical section.

**Figure 9.** Free-surface time series (left column) and their relative frequency spectra (right column) at the CP point (**a** and **b**) and at P point (**c** and **d**). Comparison between the solution of the 3-D reference model (upper plots) and the solution of the depth-integrated equation (lower plots).

**Figure 10.** Snapshots of the free surface ($\eta$) hydro-acoustic perturbation given by the 1693 Catania (Sicily) earthquake. $t = 0$ refers to the time of occurrence of the earthquake.
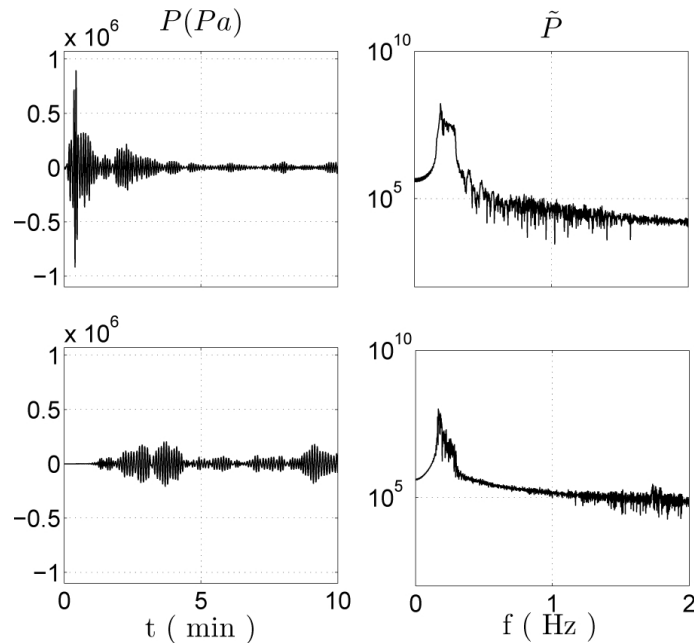
**Figure 11.** Pressure time series (left column) and their frequency spectra (right column) at Catania point (upper plots) and at Capo Passero point (lower plots), resulting from the numerical solution of the depth-integrated Eq. (5) over the whole domain.